Chapter 10

Performance

2008 JINST 3 S08005

The data used to study the performance of the LHCb detector has been obtained from detailed MonteCarlo simulation, which produces a raw data format identical to real data. The proton-proton collisions are simulated with the PYTHIA program [220]. The generated particles are tracked through the detector and the surrounding material using the GEANT package [221]. The geometry and material composition of the LHCb detector are described in detail. The detector response, resolution, noise, crosstalk, etc. have been tuned to comply with test beam results. Details about this can be found in [2].

The performance quoted in this chapter is only qualitative, for two main reasons: 1) the MonteCarlo estimations are being constantly refined due to better and more detailed description of the detector, its material, the response of the electronics, more realistic source of noise, and also due to improvements in GEANT, and 2) more importantly, the real performance will be established and understood only using the first collected data as LHC will collide beams.

In the following, a description of the procedures for the main LHCb detector tasks, i.e. tracking, vertex reconstruction, particle identification, mass reconstruction, is given.

10.1 Track reconstruction

In the track reconstruction software the hits in the VELO, the TT, the IT and the OT detectors are combined to form particle trajectories from the VELO to the calorimeters. The reconstruction algorithm aims to find all tracks in the event which leave sufficient detector hits, and not only those from b-hadron decay.

Depending on their trajectories inside the spectrometer the following classes of tracks are defined, illustrated in figure 10.1:

- **Long tracks,** traversing the full tracking set-up from the VELO to the T stations. These have the most precise momentum determination and therefore are the most important set of tracks for b-hadron decay reconstruction.
- **Upstream tracks,** traversing only the VELO and TT stations. These are in general lower momentum tracks that are bent out of the detector acceptance by the magnetic field. However, they pass through the RICH 1 detector and may generate Cherenkov photons if they have

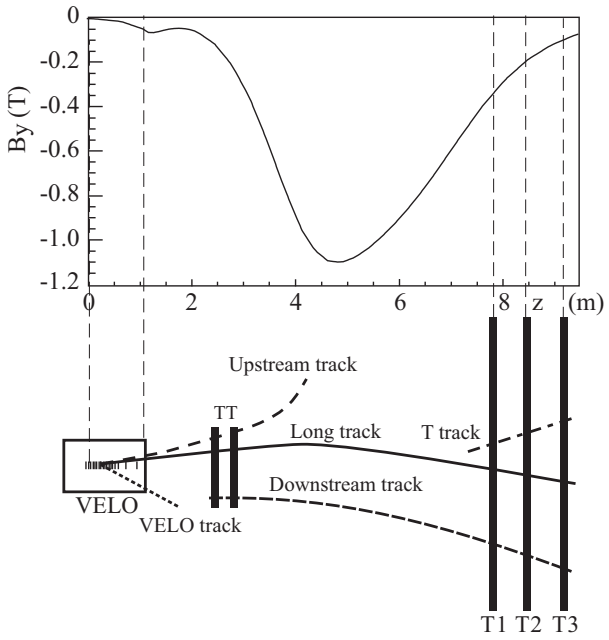

Figure 10.1: A schematic illustration of the various track types: long, upstream, downstream, VELO and T tracks. For reference the main B-field component (B_y) is plotted above as a function of the z coordinate.

velocities above threshold. They are therefore used to understand backgrounds in the RICH particle identification algorithm. They may also be used for b-hadron decay reconstruction or flavour tagging, although their momentum resolution is rather poor.

- **Downstream tracks,** traversing only the TT and T stations. The most relevant cases are the decay products of K^0_S and Λ that decay outside the VELO acceptance.
- **VELO tracks,** measured in the VELO only and are typically large angle or backward tracks, useful for the primary vertex reconstruction.
- **T tracks:** are only measured in the T stations. They are typically produced in secondary interactions, but are useful for the global pattern recognition in RICH 2.

The track reconstruction starts with a search for track *seeds*, the initial track candidates [222], in the VELO region and the T stations where the magnetic field is low. After tracks have been found, their trajectories are refitted with a Kalman filter [223] which accounts for multiple scattering and corrects for dE/dx energy loss. The quality of the reconstructed tracks is monitored by the χ^2 of the fit and the *pull* distribution of the track parameters.

The pattern recognition performance is evaluated in terms of efficiencies and ghost rates. The efficiencies are normalized to the reconstructible track samples. To be considered reconstructible, a track must have a minimum number of hits in the relevant subdetectors. To be considered as *successfully reconstructed*, a track must have at least 70% of its associated hits originating from a single MonteCarlo particle. The reconstruction efficiency is defined as the fraction of reconstructible tracks that are successfully reconstructed, and the ghost rate is defined as the fraction of

2008 JINST 3 S08005

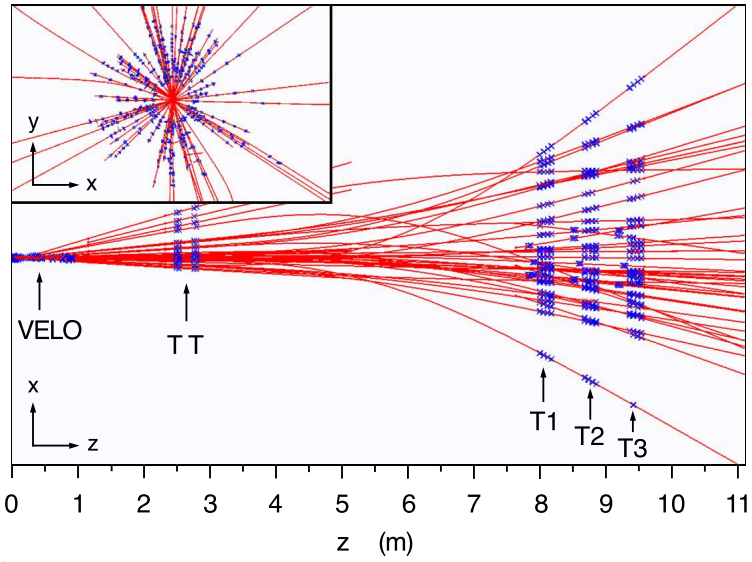

Figure 10.2: Display of the reconstructed tracks and assigned hits in an event. The insert shows a zoom in the plane (x,y) into the VELO region.

reconstructed tracks that are not matched to a true MonteCarlo particle. The results quoted in this section are obtained from a sample of $B^0 \to J/\psi K^0_S$ events.

An example of a reconstructed event is displayed in figure 10.2. The average number of successfully reconstructed tracks in fully simulated $b\bar{b}$ events is about 72, which are distributed among the track types as follows: 26 long tracks, 11 upstream tracks, 4 downstream tracks, 26 VELO tracks and 5 T tracks. The track finding performance is summarized in the following for the most important cases: the long tracks, the low momentum (upstream) tracks and K^0_S decay (downstream) tracks.

The efficiency to find as a long track the trajectory of a particle with momentum larger than 10 GeV/c is on average ~94%. The corresponding average ghost fraction is about 9%, but most ghost tracks have a low reconstructed p_T.

The momentum and impact parameter resolutions of the reconstructed long tracks are shown in figure 10.3. The momentum resolution is plotted as a function of the track momentum and is seen to be increasing from $\delta p/p = 0.35\%$ for low momentum tracks to $\delta p/p = 0.55\%$ for tracks at the high end of the spectrum. In the same figure the momentum spectrum for B decay tracks is also illustrated. The impact parameter resolution is plotted as function of $1/p_T$ of the track. The linear dependence can be parametrized as $\sigma_{IP} = 14\,\mu\text{m} + 35\,\mu\text{m}/p_T$ with p_T in GeV/c. For comparison the $1/p_T$ spectrum of B decay particles in the detector acceptance is plotted in the same figure.

The efficiency of the upstream track finding for particles with $p > 1$ GeV/c is approximately 75% with a corresponding ghost rate of 15%. The momentum resolution is only $\delta p/p \sim 15\%$, due to the small value of the total magnetic field integral in the considered region.

The efficiency for finding downstream tracks above 5 GeV/c is about 80%. Since the downstream tracks traverse most of the magnetic field, the momentum resolution is relatively good with an average of $\delta p/p = 0.43\%$ for pions originating from K^0_S decays in $B^0 \to J/\psi K^0_S$ events. In order

2008 JINST 3 S08005

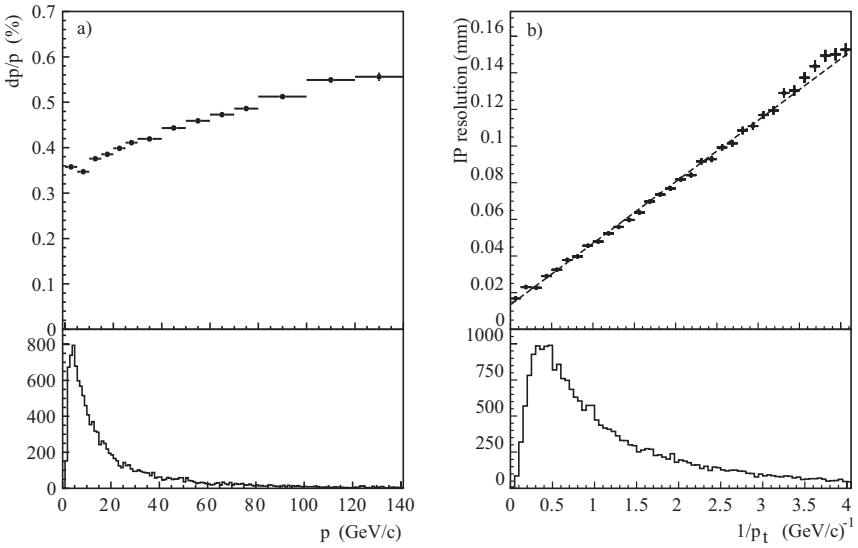

Figure 10.3: Resolution on the reconstructed track parameters at the production vertex of the track: (a) momentum resolution as a function of track momentum, (b) impact parameter resolution, calculated as the sum of the errors in the three projections added in quadrature, as a function of $1/p_{\mathrm{T}}$. For comparison, the $1/p_{\mathrm{T}}$ spectra of B decay particles are shown in the lower part of the plots.

to maintain high efficiency, the reconstruction allows for typically two or three track candidates in the TT to be linked to a single track seed in the T stations.

$\mathrm{K}^0_{\mathrm{S}}$ candidates are reconstructed through their decay to $\pi^+\pi^-$. For $\mathrm{K}^0_{\mathrm{S}}$ from $\mathrm{B}^0 \to \mathrm{J}/\psi\,\mathrm{K}^0_{\mathrm{S}}$ decays, about 25% decay inside the active region of the VELO, 50% decay outside the active region of the VELO but upstream of TT, and the rest decay after TT, and will therefore be difficult to reconstruct. The $\mathrm{K}^0_{\mathrm{S}}$ that decay outside the active region of the VELO but before TT are reconstructed using pairs of oppositely charged downstream tracks. The pions from $\mathrm{K}^0_{\mathrm{S}}$ that decay within the VELO acceptance give either a long track or an upstream track. The corresponding mass plots are shown in figure 10.4. As can be seen, there exists some combinatorial background from other tracks in the signal events, particularly for the long-upstream category, but this background can be removed by the additional requirements that are imposed when reconstructing the B meson.

10.2 Particle identification

The information from the two RICH detectors, the calorimeters and the muon system is combined for optimal identification of charged particle types $(\mathrm{e}, \mu, \pi, \mathrm{K}, \mathrm{p})$. Photons and neutral pions (γ, π^0) are identified using the electromagnetic calorimeter, where the $\pi^0 \to \gamma\gamma$ decay may be detected as two separate electromagnetic clusters or as a merged cluster.

2008 JINST 3 S08005

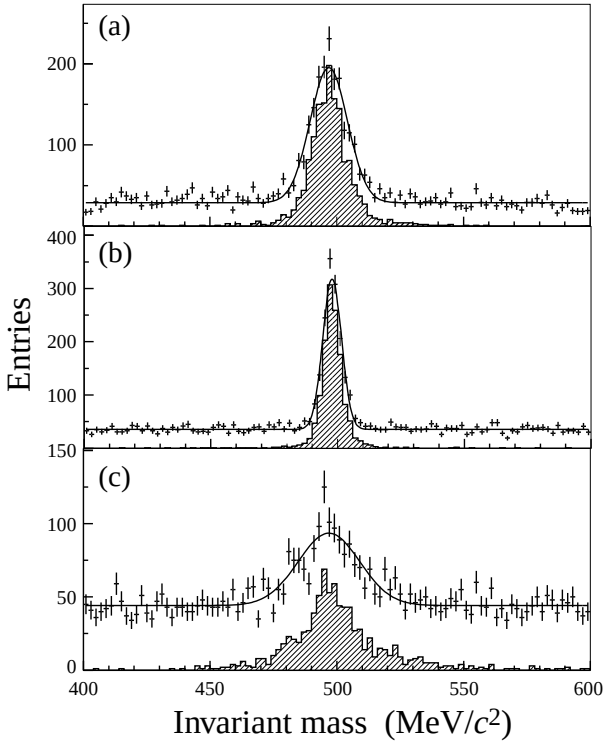

Figure 10.4: Reconstruction of $K^0_S \to \pi^+\pi^-$. The $\pi^+\pi^-$ invariant mass is shown in $B^0 \to J/\psi K^0_S$ signal events, using different categories of tracks for the pion candidates: (a) downstream-downstream, (b) long-long, (c) long-upstream. Combinations coming from true K^0_S are indicated by the shaded histograms.

10.2.1 Hadron identification

Particle identification with the RICH system is performed as follows. The baseline algorithm is based on a log-likelihood approach which matches the observed pattern of hit pixels in the RICH photodetectors to that expected from the reconstructed tracks under a given set of particle hypotheses [224]. In constructing this likelihood it is necessary to calculate the effective emission angle for all pixel-track combinations which could physically be associated through Cherenkov radiation. The likelihood is maximised by varying the particle hypotheses of each track in turn, through electron, muon, pion, kaon and proton. As the likelihood considers all found tracks in the event, and all three radiators simultaneously, the method is referred to as the *global pattern-recognition*.

The output of the global pattern-recognition is a best hypothesis for each track, and the decrease in log-likelihood when changing from this solution to another hypothesis.

The RICH system provides good particle identification over the entire momentum range. The average efficiency for kaon identification for momenta between 2 and 100 GeV/c is $\varepsilon(\mathrm{K} \to \mathrm{K}) \sim 95\%$, with a corresponding average pion misidentification rate $\varepsilon(\pi \to \mathrm{K}) \sim 5\%$. Around 30 GeV/c the identification probability is $\sim$97% and the misidentification probability $\sim$5%.

Other methods have been investigated to find the Cherenkov rings in the absence of tracking information. These include Markov chain MonteCarlo and Hough Transform techniques [225].

2008 JINST 3 S08005

Such approaches may be particularly useful in the early stages of data taking, when it may be necessary to study the performance of the RICH detector independently of spectrometer information.

For physics analyses and detector diagnostics it will be very important to understand the performance of the RICH particle identification independently of simulation studies. The dominant $D^{*\pm} \to D^0(K^-\pi^-)\pi^\pm$ decay mode will provide a very high statistics unbiased sample of pions and kaons which may be used to measure the RICH performance directly. Studies indicate that with kinematic cuts alone purities of $> 95\%$ can be achieved.

10.2.2 Muon identification

Muons are identified by extrapolating well reconstructed tracks with $p > 3\,\mathrm{GeV}/c$ into the muon stations (particles with $p < 3\,\mathrm{GeV}/c$ do not reach the muon system). Hits are searched within fields of interest (FOI) around the extrapolation point of the track in each muon station, parameterized as a function of momenta for each station and region. A track is considered as a muon candidate when a minimum number of stations (2–4 depending on momentum) have hits in their corresponding FOI. This number optimizes the resulting efficiency [226].

Using a sample of $B^0 \to J/\psi K^0_S$ the muon identification efficiency was measured to be $\varepsilon(\mu \to \mu) \sim 94\%$ with a corresponding misidentification $\varepsilon(\pi \to \mu) \sim 3\%$. The efficiency is a flat function of the momentum above $10\,\mathrm{GeV}/c$.

Discriminating variables helping to improve the muon selection purity are constructed from the comparison of slopes in the muon system and the main tracker, and from the average track-hit distance of all hits in FOI associated to the track. For each track the difference in log-likelihood between the muon hypothesis and pion hypothesis is determined, and summed with the values from the RICH and calorimeter systems (if available). By doing this the pion misidentification rate can be reduced to $\sim$1%, whilst maintaining a muon efficiency of $\sim$93% for muons above $3\,\mathrm{GeV}/c$.

The high purity that can be achieved with such cuts is illustrated in figure 10.5 where the $\mu^+\mu^-$ mass plot is shown at the first step in the analysis of $B^0_s \to J/\psi\phi$ events, taking all oppositely charged pairs of tracks from signal events that pass the muon identification requirements. The J/ψ mass peak is reconstructed with a resolution of about $13\,\mathrm{MeV}/c^2$.

10.2.3 Electron identification

The electron identification [227] is mainly based on the balance of track momentum and energy of the charged cluster in the ECAL (figure 10.6), and the matching between the corrected barycenter position of the cluster with the extrapolated track impact point.

A second estimator is related to the bremsstrahlung photons emitted by electrons before the magnet. As there is little material within the magnet, such neutral clusters are expected in a well defined position given by the electron track extrapolation from before the magnet, as illustrated in figure 10.7: if an electron radiates photons when passing through material before the magnet, a cluster with energy E_1 is seen in the ECAL. If it radiates after the magnet, the bremsstrahlung photon will not lead to a separate cluster. For electron identification the corresponding cluster energy E_2 will be compared to the track momentum $E_2 = p$, while the energy of the electron at the origin is $E_0 = E_1 + E_2$.

2008 JINST 3 S08005

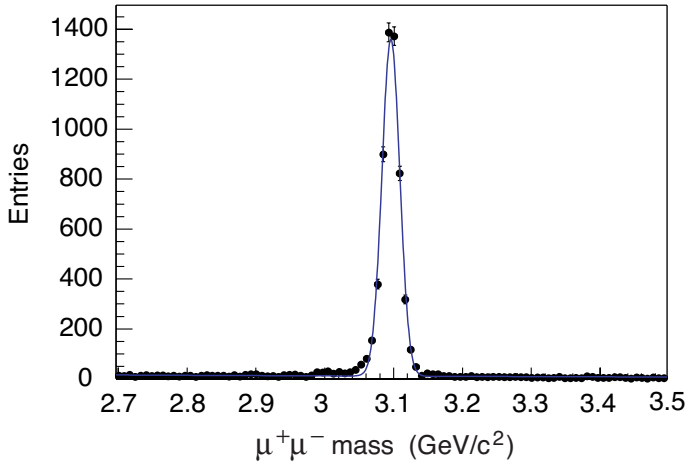

Figure 10.5: Invariant mass plots for the reconstruction of $J/\psi \to \mu^+\mu^-$ decays in $B_s^0 \to J/\psi\,\phi$ signal events.

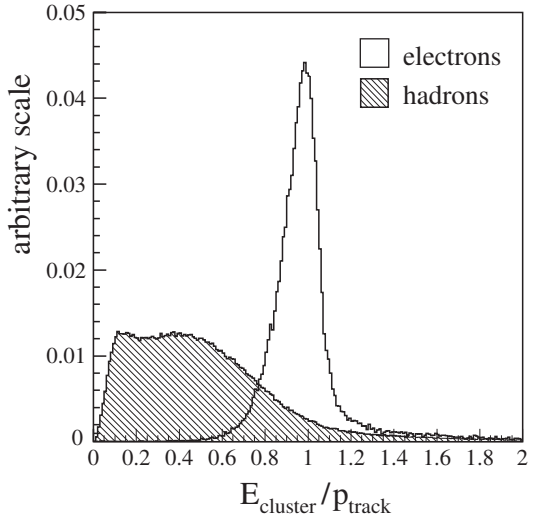

Figure 10.6: The ratio of uncorrected energy of the charged cluster in ECAL to the momentum of reconstructed tracks for electrons (open histogram) and hadrons (shaded histogram).

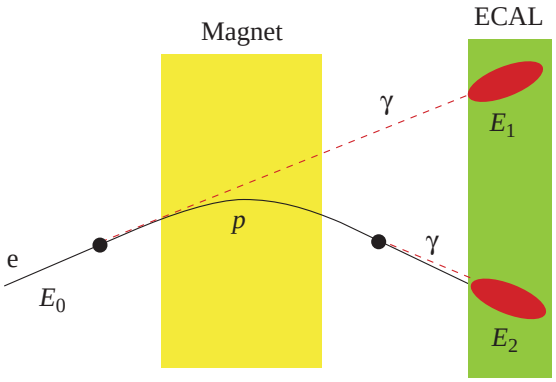

Figure 10.7: Schematic illustration of bremsstrahlung correction.

Further improvement in electron identification is obtained by using the track energy deposition in the preshower detector and the deposition of the energy along the extrapolated particle trajectory in the hadronic calorimeter HCAL.

For particle identification, the calorimeter information is combined with that from the RICH and muon detectors.

To illustrate the performance of electron reconstruction, the J/ψ mass plot for the decay $J/\psi \to e^+e^-$ is shown as open points in figure 10.8. The signal is fitted with a function plus a radiative tail, to account for the imperfect correction of bremsstrahlung. The background tracks are

2008 JINST 3 S08005

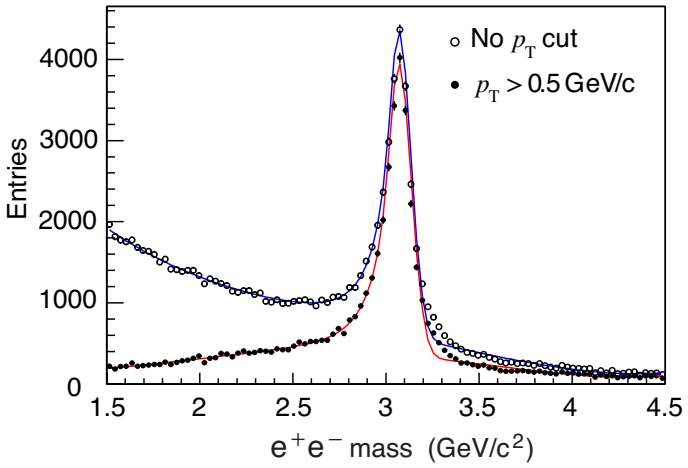

Figure 10.8: Invariant mass plots for the reconstruction of $J/\psi \to e^+e^-$ decays in $B_s^0 \to J/\psi\,\phi$ signal events, where the open points are before any p_T cut, and the solid points are after requiring $p_T > 0.5\,\text{GeV/c}$ for the $e^\pm$ candidates.

dominantly of low p_T, and can be efficiently rejected by applying the requirement $p_T > 0.5\,\text{GeV/c}$ for the electron candidates, as shown by the solid points in figure 10.8.

The average efficiency to identify electrons from $J/\psi \to e^+e^-$ decays in $B^0 \to J/\psi\,K_S^0$ events in the calorimeter acceptance is $\sim$95%. The pion misidentification fraction for the same events is 0.7%.

10.2.4 Photon identification

Photons are reconstructed and identified with the electromagnetic calorimeter, as clusters without an associated track [121, 228]. The reconstructed tracks are extrapolated to the ECAL face and a cluster-to-track position matching estimator, χ^2_γ, is calculated. Photon candidates correspond to $\chi^2_\gamma > 4$, and are clearly separated from charged particles which form a peak at a small value of χ^2_γ.

The identification of photons converted in the passive material of the apparatus after passing the magnet, e.g. in RICH 2 or in M1, is based on whether there is a hit in the SPD cell that lies in front of central cell of the ECAL cluster. Reconstructed photons from $B^0 \to K^*\gamma$ decays reach the ECAL unconverted in 69% of cases, while 31% are converted before the calorimeter. A cut on the energy deposition in the preshower detector can improve the purity of selected samples both for converted and unconverted photons [229].

10.2.5 π^0 reconstruction

The neutral pion reconstruction reported in this section is based on the study of $B^0 \to \pi^+\pi^-\pi^0$ decay channel for which the mean transverse momentum of the π^0 is about 3 GeV/c. Below this value the π^0 decays are mostly reconstructed as a resolved pair of well separated photons, while for higher p_T a large fraction of the pairs of photons cannot be resolved as a pair of clusters within the ECAL granularity. About 30% of the reconstructible π^0 from $B^0 \to \pi^+\pi^-\pi^0$ lead to a single cluster, referred to as a merged π^0.

2008 JINST 3 S08005

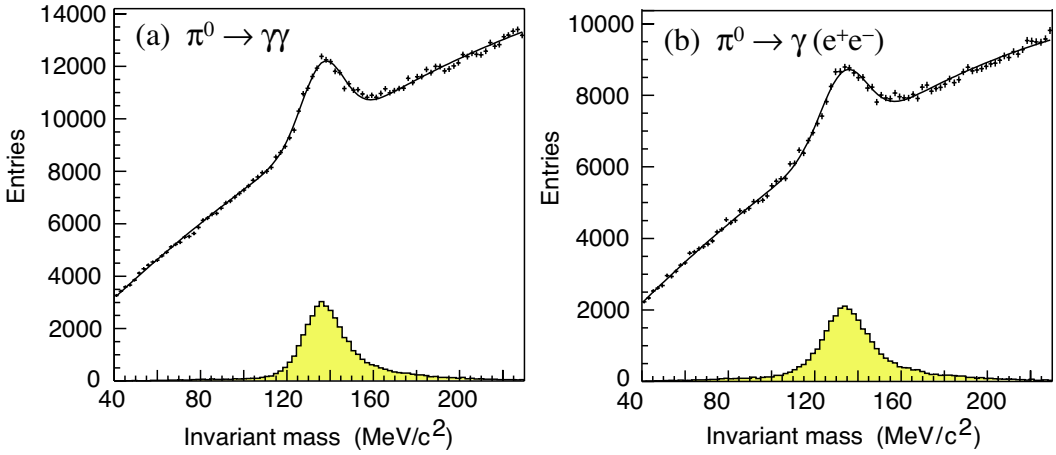

Figure 10.9: π^0 mass distributions, where (a) neither photon has converted, (b) one γ converted before the calorimeter. The conversions are identified using the SPD information. The contributions of true π^0 are indicated by the shaded histograms.

Figure 10.9 shows the mass distributions obtained in the case where both photon candidates with $p_T > 200$ MeV/c reach the calorimeter (a), and for the case that one photon converted before the calorimeter (b), where the identification of the conversion relies on the SPD signal. The distributions are fitted with the sum of a gaussian and a polynomial function to describe the combinatorial beckground. The fit results in both cases in a mass resolution for the π^0 of $\sim$10 MeV/c^2.

An algorithm has been developed to disentangle a potential pair of photons merged into a single cluster. The energy of each cell of the cluster is shared between two virtual sub-clusters according to an iterative procedure based on the expected transverse shape of photon showers. Each of the two sub-clusters is then reconstructed as coming from a photon, as for isolated photons.

The reconstruction efficiency for π^0 that give photons inside the geometrical acceptance is summarized in figure 10.10 for the resolved and merged case.

10.2.6 Expected global performance

Given the reconstruction performance described above, the global performance for the reconstruction of B decays in the LHCb detector is expected to be: a primary vertex resolution of $\sim 10\ \mu$m transverse to the beam axis and $\sim 60\ \mu$m along the beam axis; an invariant mass resolution typically in the range between 12 MeV/c and 25 MeV/c; and a proper lifetime resolution of ~ 40 fs, with a dependence on the decay channel studied.

2008 JINST 3 S08005

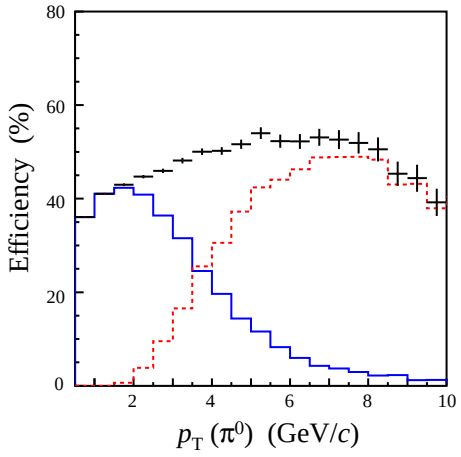

Figure 10.10: The reconstruction efficiency for π^0 decaying into photons inside the geometrical acceptance with $p_T > 200\,\text{MeV/c}$, versus the π^0 transverse momentum. The contributions from resolved and merged π^0 reconstruction are indicated by the solid and dashed histograms, respectively.

2008 JINST 3 S08005